13th International Symposium on Particle Image Velocimetry – ISPIV 2019
Munich, Germany, July 22-24, 2019

Robotic Volumetric PIV measurements of a full-scale swimmer's hand

Joris van den Berg[1]*, Constantin Jux[1], Andrea Sciacchitano[1], Willem van de Water[2], Jerry Westerweel[2]

Delft University of Technology,
[1]Department of Aerospace Engineering - Aerodynamics,
[2]Department of Mechanical Engineering - Fluid Dynamics,
Delft, The Netherlands

* j.vandenberg-6@student.tudelft.nl

Abstract

The flow field around a full-scale swimmer's hand model with varying thumb positions is investigated by robotic volumetric PIV. The experiment is conducted in the Open Jet Facility wind tunnel at TU Delft at 15 m/s. Quantitative flow field information is constructed with 3D-PTV in a 120 liter volume, encompassing the full hand and arm. The effect of spatial resolution on the time-averaged flow field is investigated. A large-scale recirculating wake behind the hand is accurately identified at a linear bin size of 20 mm whereas the accelerated flow between individual fingers can only be resolved at bin sizes below 10 mm where 5 mm results in a statistically unconverged velocity field. The influence of the thumb is limited to one side of the hand where its presence results in a larger stagnated region in front and larger wake behind the hand, depending on the thumb position. Closing the thumb strengthens the recirculation but results in a smaller velocity deficit downstream, suggesting a smaller propulsive force generation which is considered disadvantageous in competitive swimming.

1 Introduction

Swimming is one of the few sports where the direct interaction of the human body with a fluid is used as means of propulsion. Since Schleihauf (1979) first reported on the forces on a swimmer's hand and arm in terms of lift and drag, advances in numerical and experimental simulations have added to the understanding of the generation of these forces and how they are influenced by hand orientation and configuration. It is acknolwegded by reviewers as Takagi et al. (2015) and Van Houwelingen et al. (2017a) that fully resolved flow simulations around the hand could aid in further optimizing the propulsive force. However, most of these numerical results must still be validated in experiments. Some studies such as Matsuuchi et al. (2009) and Takagi et al. (2014) do manage to capture quantitative flow information in experimental conditions by means of PIV. However, they are limited to a 2D measurement plane and do not have sufficient spatial resolution to resolve the influence of for example individual fingers; Maintaining a small finger spread is believed to be a small but a noticable improvement in propulsive force (Van Houwelingen et al., 2017b). Takagi et al. (2014) did show by means of 2D2C PIV the global, unsteady and likely vortex driven flow around the hand of a swimmer in a water channel. Though adding to the understanding of propulsive force generation, the variation in fluid mechanics with different hand configurations is not investigated.

This work experimentally investigates the influence of the position of the thumb on the fluid mechanics around the hand by employing the recently developed Coaxial Volumetric Velocimiter (CVV) by Schneiders et al. (2018) in a robotic fashion as introduced by Jux et al. (2018). This Robotic Volumetric Velocimeter (RVV) has simplified the operation and set-up of a tomographic PIV system and allows for measurement around complex shapes in terms of optical access, like the fingers on a human hand. So far, the RVV system has been employed for measurements of the flow around a full-scale cyclist (Jux et al., 2018), a 1:12 scale model of a turboprop aircraft (Sciacchitano et al., 2018) and the large-scale flow structure of a 0.3 m span flapping-wing MAV (Martínez Gallar et al., 2018). To be investigated is the ability of the RVV system to resolve flow scales as small as 5 - 10 mm, the size of individual fingers and the space between them.

The approach taken is wind tunnel testing of the two extreme positions of the thumb: closed-thumb (touching the hand) and open-thumb (away from the hand) which is described in section 2. The investigation includes a discussion on the RVV capabilities to identify small flow features and presents a first insight into the optimal thumb position for increased propulsion in swimming in section 3.

2 Setup of the experiment

The experimental investigation involves a custom designed arm on which two different hand models are mounted. The assembly is tested in a large open-jet wind tunnel with the RVV system set up such that the flow field all around the model can be captured. At the same time, surface pressure readings and aerodynamic loads are acquired (though they are not discussed in this paper). The following sections further specify each component of the setup.

2.1 Wind tunnel

The wind tunnel used is the Open Jet Facility of TU Delft. This closed-loop atmospheric wind tunnel has a large test chamber and a 3:1 contracting nozzle with an exit cross-section of $2.85 \times 2.85\,\mathrm{m}^2$. The jet speed can be regulated from 5 to 35 m/s and has a turbulence intensity of 0.5 % (Lignarolo et al., 2014). The wind tunnel is equipped with a heat exchanger that maintains the circulating air at a constant temperature of $20^{\circ}C$.

The hand model is rigidly mounted on a balance such that it just sits clear off and above a large ground plate. The RVV system is mounted on a profiled beam, 75 cm to the side and 25 cm downstream of the model as shown in Fig. 1. This position is a compromise between the intrusiveness of the beam and robot arm, the requirement to image from the top with the given CVV field of view and the reach of the robot arm.

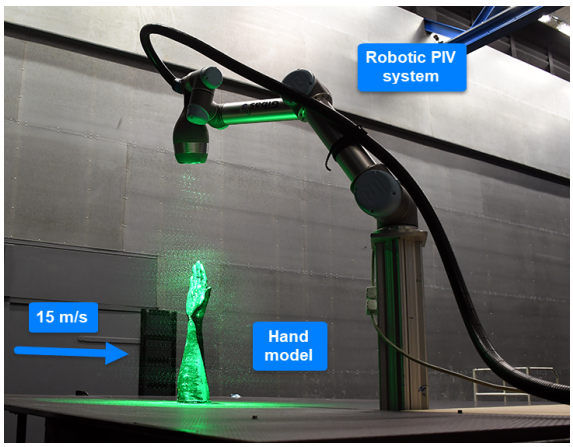

Figure 1: The model mounted through the groundplate and the RVV system imaging from the top down; The open jet exit nozzle is just out of frame to the left.

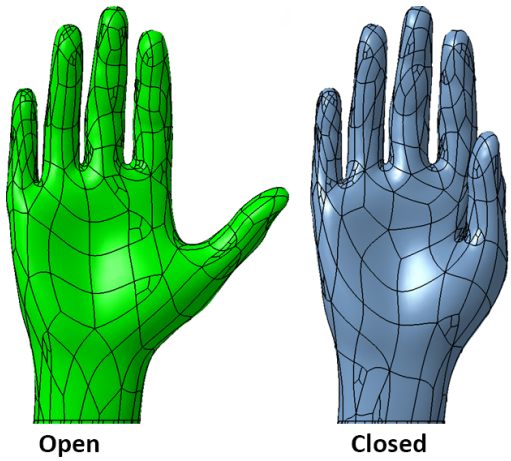

Figure 2: Open-thumb and closed-thumb model geometry, the width of the palm is 10 cm.

2.2 Hand model

The digital surface of the hand and arm are generated with the MakeHuman (2018) software. The base-shape of the hand is chosen to be equal to earlier experiments done on finger spreading (see Van Houwelingen et al., 2017b). The position of the thumb is subsequently modified with the 3D-modeling software Blender and pressure tappings are added to the resulting model with the CAD software CATIA. Two different hand models as shown in Fig. 2 are manufactured my means of SLS 3D-printing: One with the thumb fully opened and one with the thumb fully closed.

The size of the hand-arm assembly is kept at a full human scale with an elbow to finger-top distance of 50 cm and a hand palm width of 10 cm. Maintaining the model at true human scale dictates a change in free

stream velocity between wind tunnel measurements and typical swimming conditions in water to achieve flow similarity. The increase in kinematic viscosity from $25°C$ water to $20°C$ air means setting the wind tunnel speed at 15 m/s in order to achieve a typical Reynolds number of 100,000 based on the width of the hand. That corresponds to a speed in water of 1 m/s which is roughly in the middle of the velocities seen by a hand propelling through water (Van Houwelingen et al., 2017a).

2.3 Robotic Volumetric Velocimeter

A detailed description of the components of the RVV system is given by Jux et al. (2018) but is briefly repeated here for the sake of completeness. The RVV system is based on the robotic manipulation of a LaVision Coaxial Volumetric Velocimeter probe. The latter consists of four CMOS cameras (10 bits, 4.8 μm pixel pitch) mounted together at a low tomographic aperture of 4°. A Quantronix Darwin Duo Nd:YLF laser (527 nm wavelength, 2×25 mJ pulse energy @ 1 kHz) is routed through an optical fiber to the CVV head where it is expanded into an illuminated cone-shaped volume. The cameras are set to continuous recording of images of 640×476 pixels at 821.7 Hz and aquire 10,000 images in sequence.

The dimensions of the cone shaped volume of 32 liters are shown in Fig. 3. Robotic manipulation by the UR5 robotic arm enables the stitching together of these individual cones. Their positions are chosen such that there is sufficient overlap at the sides of the cones and the full area of interest around the hand is captured. Regions such as the space between the thumb and individual fingers that would otherwise be difficult to see with conventional tomographic PIV-systems can be captured by carefully tuning the position of the cones. In order to measure the flow between the fingers, the RVV system is oriented to acquire images from the top of the hand, looking downwards. For the lower part of the arm the images are acquired from the side. The full field around the model is captured with 15 cones with a total volume of approximately 120 L.

The flow is seeded with helium-filled soap bubbles generated by a seeding rake that is placed in the settling chamber of the wind tunnel. The gas and fluid supply are controlled through a LaVision Fluid Supply Unit. The seeding rake consists of 10 airfoils with 20 bubble generating nozzles each. In total they nominally produce one million bubbles per second with a diameter between 0.3 and 0.6 mm (Faleiros et al., 2019). The resulting bubble concentration C_{HFSB} around the hand is estimated from the seeder area of $1.0 \times 0.5\,\mathrm{m}^2$, the settling chamber speed 5 m/s and a 50 % seeder functionality as

$$C_{HFSB} = \frac{\dot{N}}{\dot{V}} = \frac{50\% \cdot 10^6}{5 \cdot 1.0 \cdot 0.5} = 2.0 \cdot 10^5 \frac{\text{tracers}}{\text{m}^3} = 0.20 \frac{\text{tracers}}{\text{cm}^3} \tag{1}$$

where $\dot{N}$ is the effective bubble production rate and $\dot{V}$ the volume flow rate through the seeder. The concentration results in 0.02 ppp given the measurement volume and CVV camera resolution. The actual amount of reconstructed particles is around 1200 for each cone of which 700 are tracked over multiple time steps.

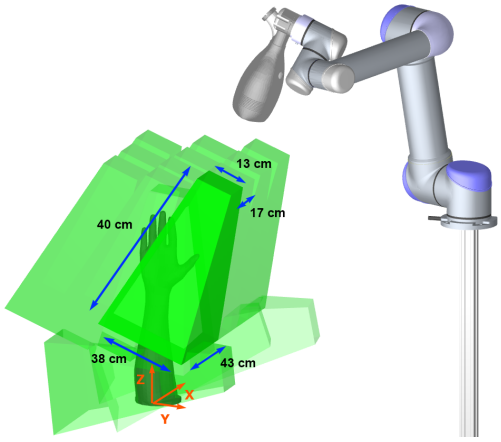

Figure 3: Devision of the total volume of 120 L devided into 15 overlapping subvolumes of 32 L; 12 oriented top down to capture the flow around the hand and 3 horizontal volumes encompassing the lower portion of the arm.

2.4 Procedure & data reduction

The procedures from calibration to particle tracking (as described by Jux et al., 2018) are done in LaVision DAVIS10 software. The complete investigation consists of measuring the two hand models at yaw angles of 0°, $\pm 10^\circ$ and $\pm 40^\circ$. At each angle the 15 RVV cones are captured next to balance and pressure tap readings. The raw images are pre-processed with a temporal high-pass filter (Sciacchitano and Scarano, 2014) to remove reflections. The images are then analysed with the Shake-the-Box algorithm (Schanz et al., 2016), which performs Lagrangian Particle Tracking to retrieve the tracer velocities along their trajectories. The result is a collection of particle tracks with velocity information at scattered locations throughout the domain.

This Lagrangian description is then averaged in space and time within cubic bins width edge size dependent on the statistical convergence of the particle velocities; Sizes between 5 mm and 40 mm will be discussed in the results. First, the velocity information is filtered within a bin as erroneous tracks could be present due to for example ghost particles, seeding imperfections and remaining background noise. The filtering process consists of two steps: Step one is a filter with a large pass-through band of all particles with velocity components that do not deviate more than 7.5 m/s from the local median. The second step is a statistical filter that retains particles with velocities within the range of the local mean ± 2 standard deviations.

Then the polynomial least-squares regression procedure as suggested by Agüera et al. (2016) is employed to average the velocity information: To all valid tracks within a bin, a first-order linear regression of velocity is made based on the distance of a particle to the bin center. The value of this regression at the center of the bin is then taken to be the final bin value. The concentration of tracer particles and therefore the number of particle observations affect the statistical convergence of the bin value, influencing the achievable spatial resolution. Comparisons are made in the next section on the bin sizes of 40 to 5 mm with 75 % overlap resulting in a vector pitch of 10 mm to 1.25 mm respectively.

3 Results and discussion

The possibility of an optimal thumb position in swimming deals with the case where the propulsive force in the direction of swimming is the largest. This question could simply be answered by the measured aerodynamic loads on the model, but the underlying change in flow characteristics are then only speculated on. The analysis of the flow fields under yaw angles and force information of the various cases is ongoing at the point of writing this text. However, from the surface pressure measurements the prelimiary conclusion is that there exists a larger pressure difference across the hand with the thumb closed (a conclusion supported by the work of Takagi et al., 2001) which would result a higher propulsive force. This section presents the considerations taken on the spatial resolution of the RVV system followed by a global description of the time-averaged flow field around the hand and arm. A comparison is then presented between the open-thumb and closed-thumb cases for zero yaw, where the flow is perpendicular to the palm of the hand, as this is the condition where the largest force (difference) is expected.

3.1 Measurement spatial resolution

In this section, the effect of linear bin size on the spatial resolution of the measured flow around the swimmers hand is analysed. The random error on the time-averaged velocity field is known to decrease with the square root of the number of particles within a bin (Sciacchitano and Wieneke, 2016). The statistical convergence of the time-averaged data can be assessed by considering various bin sizes and observing the resulting flow field quantities. Figure 4(a) shows the velocity component U on a plane parallel to the ground at mid-thumb height. At a linear bin size of 20 mm, the wakes of the thumb and the main hand are clearly identified. Figure 4(b) shows U and the amount of particles in the bin along a line in y. From this, one observes that decreasing the linear bin size by a factor of two to 10 mm yields no significant change in U in the main wake but does yield increased accuracy in the wake of thumb: The minimum observed velocity lowers by 16 % from 7.3 to 6.1 m/s. With a 10 mm bin size, for most locations along y the number of detected particles is above 100 and comparable to earlier RVV experiments (e.g. Jux et al., 2018). Decreasing the linear bin size by another factor of two to 5 mm, increasing the spatial resolution and bringing the vector pitch to 1.25 mm, seems less desirable since around the thumb it results in less than 10 particles per bin. Additionally the value of the reverse velocity in the main wake exhibits fluctuations due to lack of statistical convergence. To demonstrate the capability of the RVV system to resolve the flow between the individual fingers, a line in x through the small gap between the middle and ring finger is considered in Fig. 5.

A particle travelling through this gap should experience an acceleration as hypothesised by Van Houwelingen et al. (2017b). Only for the 10 mm bin size this velocity peak is observed. Larger bin sizes possibly capture low velocity particles from the immediate wake behind the fingers and falsely report a low bin velocity as result. Considerations as these are relevant when analyzing small geometry and flow features. A bin size of 20 mm is maintained throughout the next sections where the focus is on the comparison of the large-scale flow structures in the wakes of the two hand models with open- and closed-thumb.

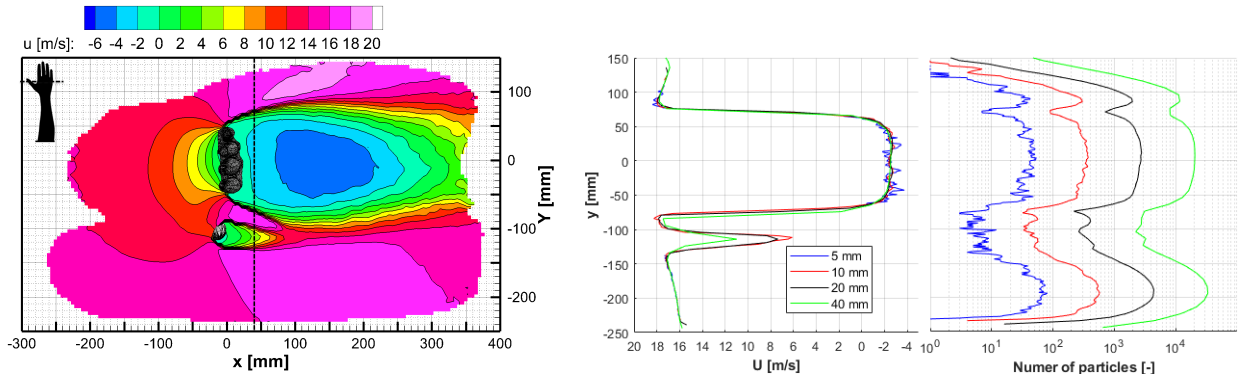

(a) U in a xy-plane at $z = 390$ mm, with a bin-size of 20 mm and 5 mm vector pitch.

(b) U over the interogation line in y at $x = 40$ mm for decreasing bin sizes.

Figure 4: Streamwise velocity U for open-thumb on a plane perpendicular to the hand at mid-thumb height and over a single line on that plane with varying bin sizes.

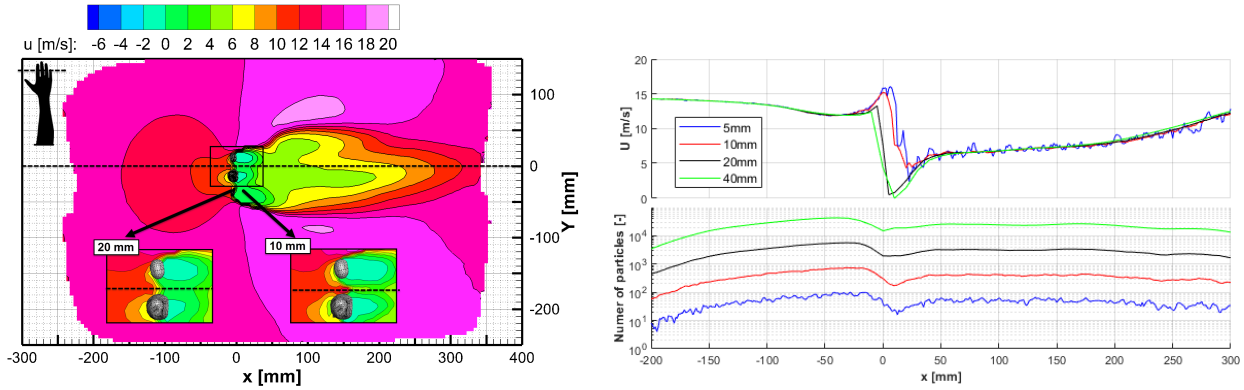

(a) U in a xy-plane at $z = 470$ mm. with a bin-size of 20 mm and vector pitch of 5 mm.

(b) Streamwise velocity over the interogation line in x at $y = 0$ mm and $z = 390$ mm for decreasing bin sizes.

Figure 5: Streamwise velocity U for open-thumb on a plane perpendicular to the hand at finger top height and over a single line on that plane with varying bin sizes.

3.2 Global velocity distribution

The open-thumb case at zero yaw is used to present the global flow features. The RVV system is able to record sufficient tracers all around the hand and the flow field is reconstructed using the 15 separate sub-volumes. Figure 6 contains streamlines around the model as determined by integration through the bins. From such a 3D visualization the major features can be immediately identified: a partially recirculating wake behind the hand and arm with accelerated flow around it. This section discusses the field in more detail.

From the streamlines it appears that the wake behind the arm is less structured than that of the hand where a recirculating pattern is observed (even visually during the measurements). Confirmation is found by considering the vertical slice at the middle of the model as shown in Fig. 7. It shows the in-plane streamlines plotted onto the streamwise velocity and in the adjacent plot the velocity fluctuations within the bin. The circulation is predominantly vertical and upwards directly behind the hand with a maximum reverse component at $z = 350\,\text{mm}$ of approximately $-7\,\text{m/s}$. Downstream of the bottom arm no obvious pattern is observed and fluctuations are a factor two larger than in the upper wake. The jets through the fingers as discussed in the previous section interact with the upper wake rotation, seemingly feeding the large-scale recirculation.

Figure 8 similarly shows a horizontal slice of the field. Both the main hand and thumb wakes are separately identified with accelerated flow in between. From the asymmetry around the hand centerline it is observed that the thumb locally influences the field: Upstream of the hand at $x = -50\,\text{mm}$, the stagnated flow region onto the hand palm extends in the direction of the thumb. Directly downstream at $x = 50\,\text{mm}$ the accelerated flow seems to keep the main wake more compact. Further downstream at $x = 150\,\text{mm}$, the wake of the thumb interacts with the main wake shear layer resulting in a less steep velocity gradient between the wake and the surrounding flow.

It has to be noted that the present study is an idealised simulation of time-averaged measurements on a steady model. Force analysis in other studies (e.g. Gomes and Loss, 2015) show significant variations between steady and unsteady conditions. The present study is however a first step in understanding the 3D structure of the flow field around a swimmer's hand.

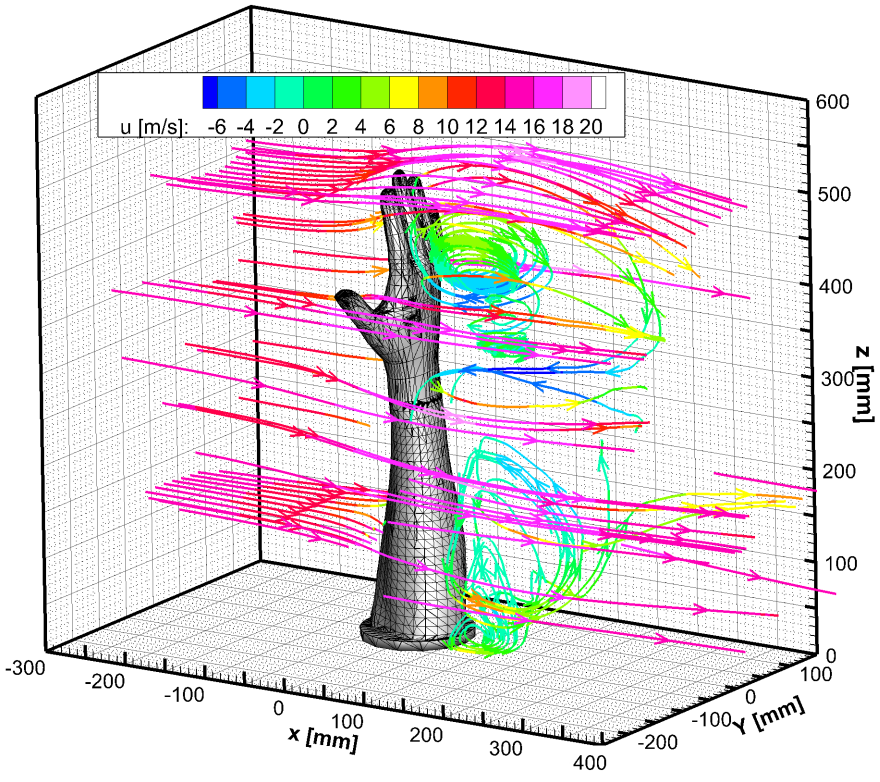

Figure 6: Streamlines colored by the streamwise velocity visualise the re-circulating structure in the wake of the open-thumb hand.

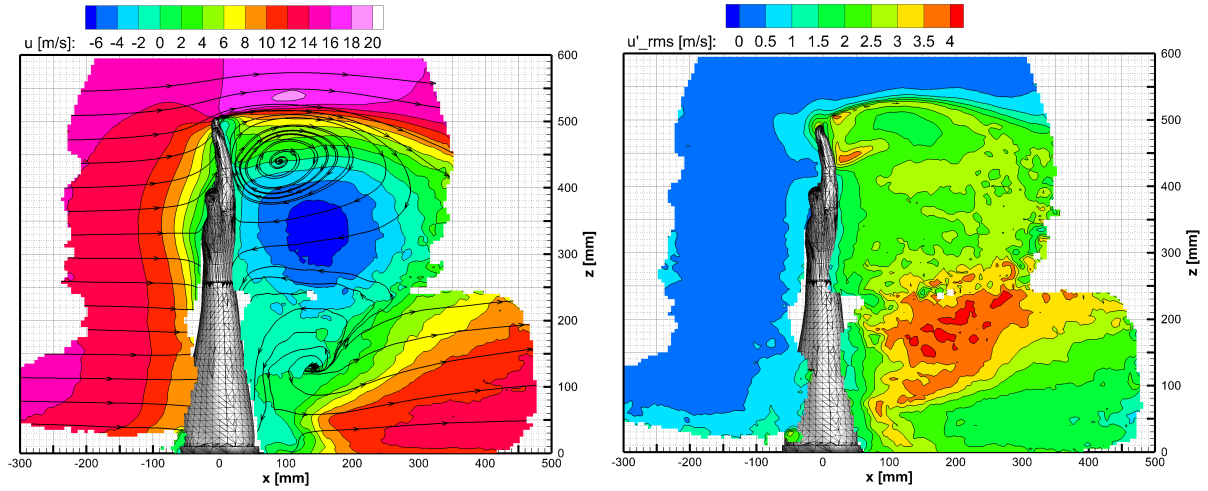

Figure 7: Side view of the streamwise velocity U (left) and its fluctuations U'_{rms}(right) on a xz-plane at $y = 0$.

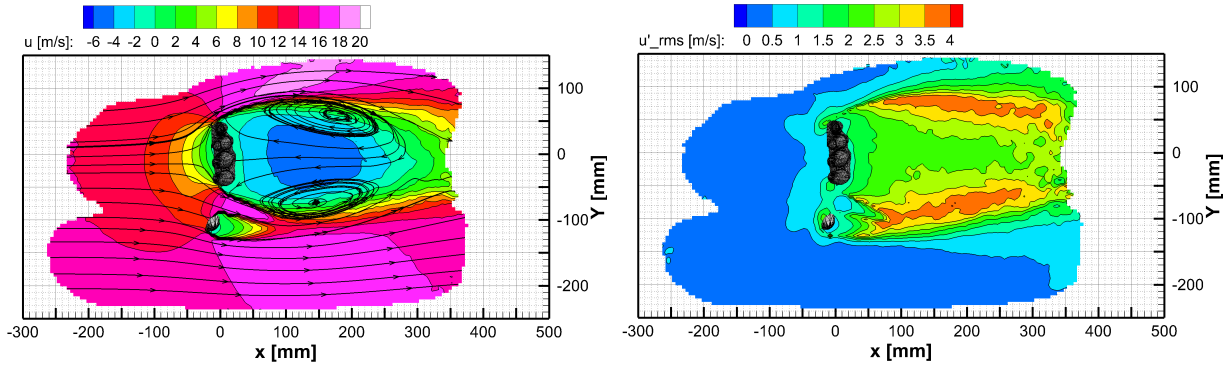

Figure 8: Top view of the streamwise velocity U (left) and its fluctuations U'_{rms} (right) on a xy-plane at $z = 390\,\text{mm}$.

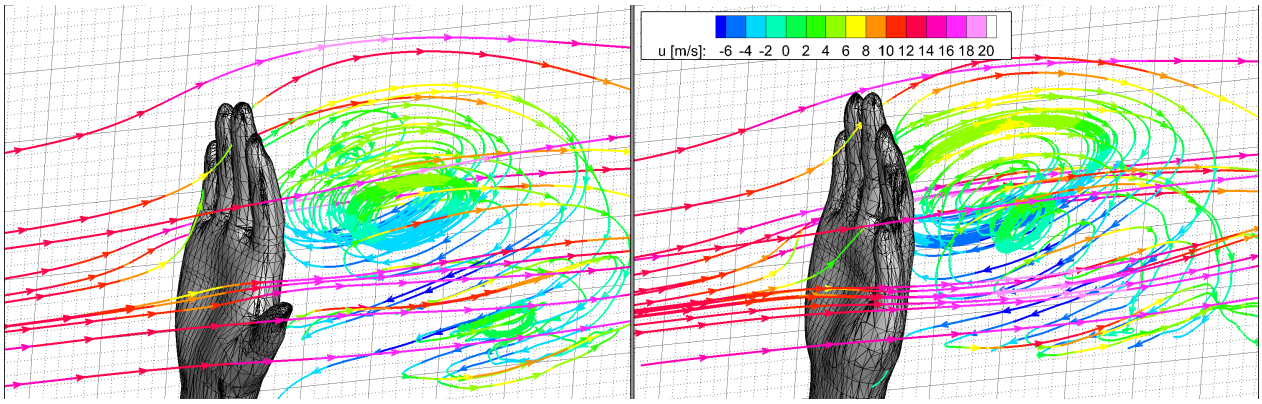

Figure 9: Detailed view of streamlines colored by U for the thumb open (left) and closed (right) hands.

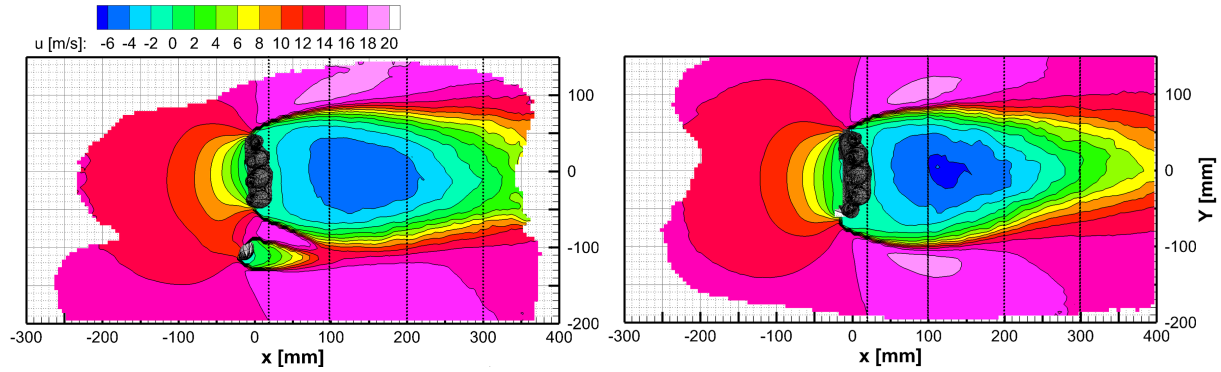

(a) U for thumb open (left) and closed (right), black lines indicate the interrogation lines for Fig. 11.

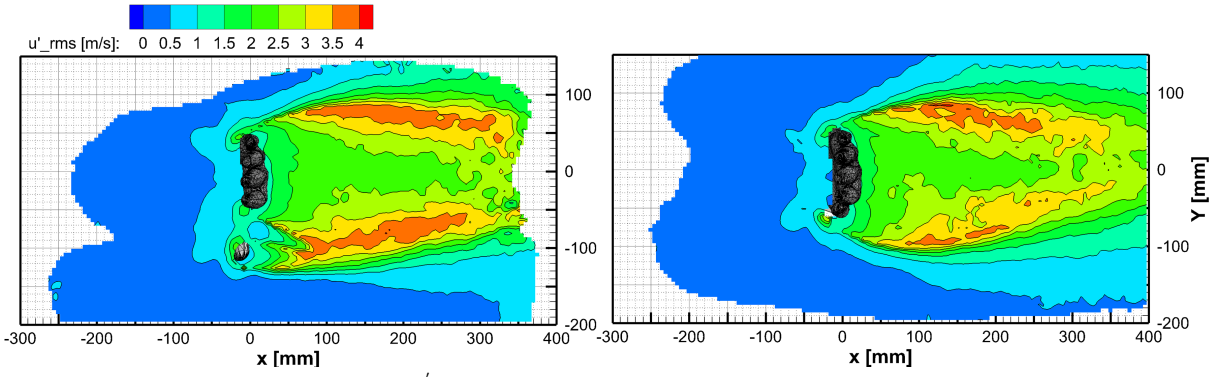

(b) U'_{rms} for thumb open (left) and closed (right).

Figure 10: Comparison of the streamwise velocity U (**a**) and U'_{rms} (**b**).

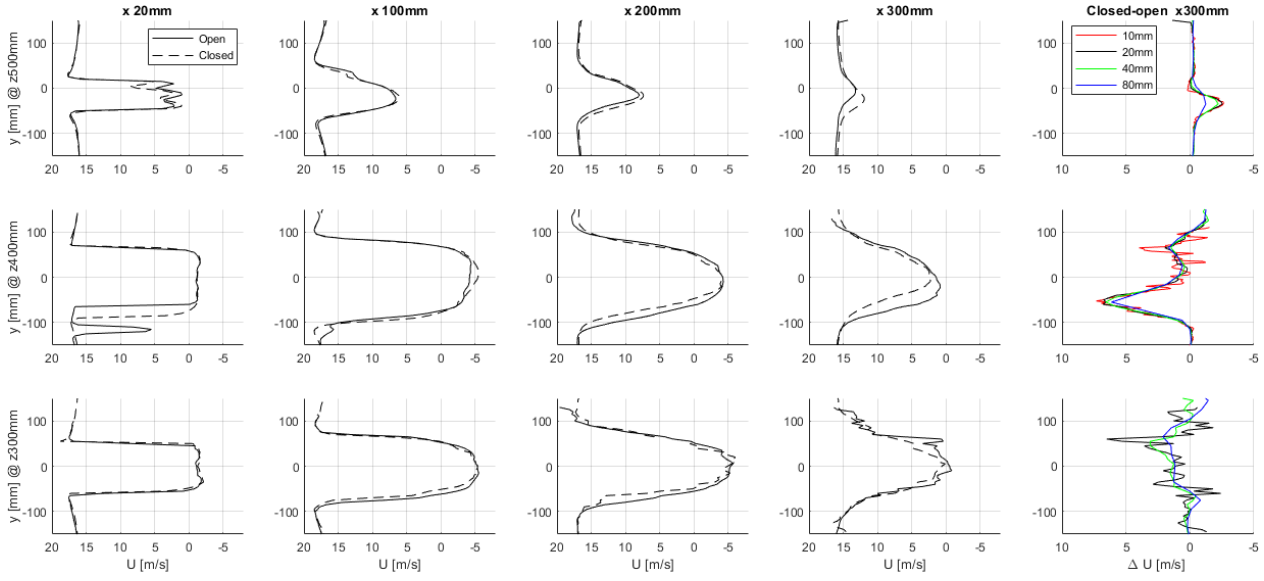

Figure 11: Streamwise velocity for the open-thumb and closed-thumb wake on the $z = 390\,\text{mm}$ plane at various x locations. The last column shows the difference in U velocity at $x = 300\,\text{mm}$ of the closed-thumb to open-thumb configuration for different bin sizes.

3.3 Comparison of two hand configurations

A streamline comparison between the open- and closed-thumb cases under zero yaw is shown in Fig. 9.

Qualitatively the biggest difference when closing the thumb follows from the oncoming flow that previously passed in between thumb and hand palm: Such flow is now forced around the thumb resulting in a stronger curvature and increased size of the stagnating region on the hand palm close to the thumb as visible in Fig. 10(a). The shear layers shown in the bottom two slices of U'_{rms} indicate less fluctuations behind the thumb, relative to the other side of the hand. The circulating wake is observed in the top slices for both cases but appears stronger at closed-thumb, as judged by the higher values of reversed flow at thumb height. The size of this rotating structure also appears smaller, more concentrated as judged from the size of the wake.

Quantitatively, Fig. 11 compares the value of U along y at three heights behind the hands (finger tips at $z = 500\,\text{mm}$, thumb at $z = 400\,\text{mm}$ and the wrist at $z = 300\,\text{mm}$). Directly behind the hand, the closed-thumb configuration seems to exhibit a slightly larger velocity deficit. However the velocity deficit further downstream at $x = 300\,\text{mm}$ is considered a better indicator for a potential difference in propulsive force (drag) due to recovery of the pressure in the wake to ambient values (Terra et al., 2017). There, at the height of the thumb, the closed-thumb case actually shows a smaller velocity deficit. At the top of the wake this is the opposite: The closed-thumb shows a slightly larger deficit. At the level of the wrist however, the difference is less clear. This level is the most distant from the CVV head and at the lowest point of the upper measurement volumes where particle detection is low. Here the default 20 mm bin size appears not converged; The last column of Fig. 11 shows that the difference in U at 20 mm is too noisy. At larger bin sizes (40 and 80 mm), better convergence is obtained, but the velocity profiles appear smoothed due to spatial modulation in the averaging process. As a consequence, the difference between the velocity profiles appears smaller, in particular in the top part of the hand wake. It is clear however that also at wrist height the wake of the closed-thumb presents a smaller velocity deficit.

Analysing U over single lines does not lead to a quantitative estimation for the hand propulsive force, but a larger wake deficit does mean more momentum transfer to the hand and thus a larger propulsive force. Apart from a slightly smaller deficit at the height of the fingers, the open-thumb orientation shows the largest deficit throughout the wake. This hints towards a larger force generation and swimming with an open thumb would thus be beneficial for increased speed, interestingly opposite to the conclusion from the surface pressure measurements.

4 Conclusion

The RVV system is successfully used to study the fluid dynamics behind a life-sized swimmers hand. The relatively simple operation of the RVV system allows for an elaborate investigation of two thumb positions of which the first results are presented in this text. The models are tested in a large open-jet wind tunnel where force, surface pressure and volumetric Lagrangian Particle Tracking data are obtained for the two extreme thumb positions under various yaw angles. The robotic operation of the CVV probe is essential to capture the full 3D-3C flow field all around the model.

Spatial and temporal ensemble averaging of the particle tracking data influences the interpretation of the resulting flow field: A 20 mm bin size with a 5 mm vector pitch is sufficient for identification of the larger features in the hand's wake and flow around the thumb. However, utilizing the good optical access capabilities of the RVV system to observe flow between individual fingers requires an increase in spatial resolution and a bin size of 10 mm for convergence. Sufficient statistical convergence depends on the amount of tracked particles which is influenced by various factors such as the flow dynamics, seeder system and available resources like hard disk and RAM storage space which limit the total number of images. Given a finite amount of tracked particles, a suggestion is to perform the ensemble averaging on (locally) refined bins of which the level of refinement is adjusted for convergence depending on the number of tracked particles and their velocity distributions.

The wake behind the arm is less structured and smaller than that of the hand. Behind the hand a large recirculating structure is observed with reversed flow velocities up to 45 % of the free stream magnitude. The influence of the thumb seems to be limited locally to its side of the hand. In the open-thumb position the wake of the thumb is observed to interact with the main wake of the hand, closing the thumb increases the strength of the re-circulation and initially widens the main wake. However the main wake does recover sooner and apart from a small portion at the top of the wake, the closed-thumb configuration shows a smaller velocity deficit hinting towards a lower propulsive force. Further investigation into the flow fields with balance and/or surface pressure measurements under non-zero yaw should provide a more elaborate insight into the optimal thumb position in swimming.

References

Agüera N, Cafiero G, Astarita T, and Discetti S (2016) Ensemble 3D PTV for high resolution turbulent statistics. *Measurement Science and Technology* 27:124011

Faleiros DE, Tuinstra M, Sciacchitano A, and Scarano F (2019) Generation and control of helium-filled soap bubbles for PIV. *Experiments in Fluids* 60:40

Gomes LE and Loss JF (2015) Effects of unsteady conditions on propulsion generated by the hand's motion in swimming: a systematic review. *Journal of Sports Sciences* 33:1641–1648

Jux C, Sciacchitano A, Schneiders JFG, and Scarano F (2018) Robotic volumetric PIV of a full-scale cyclist. *Experiments in Fluids* 59:74

Lignarolo L, Ragni D, Krishnaswami C, Chen Q, Ferreira CS, and van Bussel G (2014) Experimental analysis of the wake of a horizontal-axis wind-turbine model. *Renewable Energy* 70:31–46

MakeHuman (2018) MakeHuman software version 1.1.1. Obtained from `http://www.makehumancommunity.org`

Martínez Gallar B, Van Oudheusden BW, Sciacchitano A, and Karásek M (2018) Large-scale flow visualization of a flapping-wing micro air vehicle. in *Proceedings 18th International Symposium on Flow Visualization*

Matsuuchi K, Miwa T, Nomura T, Sakakibara J, Shintani H, and Ungerechts B (2009) Unsteady flow field around a human hand and propulsive force in swimming. *Journal of Biomechanics* 42:42–47

Schanz D, Gesemann S, and Schröder A (2016) Shake-the-box: Lagrangian particle tracking at high particle image densities. *Experiments in Fluids* 57:70

Schleihauf RE (1979) A hydrodynamic analysis of swimming propulsion. in *Swimming III. Proceedings of the Third International Symposium of Biomechanics in Swimming, University of Alberta, Edmonton, Canada*. pages 70–109. University Park Press, Baltimore

Schneiders JFG, Scarano F, Jux C, and Sciacchitano A (2018) Coaxial volumetric velocimetry. *Measurement Science and Technology* 29:065201

Sciacchitano A, Giaquinta D, Schneiders JFG, Scarano F, van Rooijen B, and Funes D (2018) Quantitative flow visualization of a turboprop aircraft by robotic volumetric velocimetry. in *Proceedings 18th International Symposium on Flow Visualization*

Sciacchitano A and Scarano F (2014) Elimination of PIV light reflections via a temporal high pass filter. *Measurement Science and Technology* 25:084009

Sciacchitano A and Wieneke B (2016) PIV uncertainty propagation. *Measurement Science and Technology* 27:084006

Takagi H, Kurashima A, Shimizu Y, and Sanders R (2001) Effect of thumb abduction and adduction on hydrodynamic characteristics of a model of the human hand. in *Biomechanics symposia 2001*. University of San Francisco

Takagi H, Nakashima M, Sato Y, Matsuuchi K, and Sanders RH (2015) Numerical and experimental investigations of human swimming motions. *Journal of Sports Sciences* 34:1564–1580

Takagi H, Shimada S, Miwa T, Kudo S, Sanders R, and Matsuuchi K (2014) Unsteady hydrodynamic forces acting on a hand and its flow field during sculling motion. *Human Movement Science* 38:133–142

Terra W, Sciacchitano A, and Scarano F (2017) Aerodynamic drag of a transiting sphere by large-scale tomographic-PIV. *Experiments in Fluids* 58:83

Van Houwelingen J, Schreven S, Smeets JB, Clercx HJ, and Beek PJ (2017a) Effective propulsion in swimming: Grasping the hydrodynamics of hand and arm movements. *Journal of Applied Biomechanics* 33:87–100

Van Houwelingen J, Willemsen DH, Kunnen RP, van Heijst GF, Grift EJ, Breugem WP, Delfos R, Westerweel J, Clercx HJ, and van de Water W (2017b) The effect of finger spreading on drag of the hand in human swimming. *Journal of Biomechanics* 63:67–73